PHYSICAL REVIEW B VOLUME 32, NUMBER 6 15 SEPTEMBER 1985

Conductivity, plasmon, and cyclotron-resonance anomalies in Si(100) metal-oxide-semiconductor systems

A. Gold
Physik-Department (E 16), Technische Universität München, D-8046 Garching bei München, Federal Republic of Germany
(Received 18 January 1985)

Due to charged-impurity scattering and surface-roughness scattering, anomalies are found in the conductivity of Si(100) metal-oxide-semiconductor systems. We propose a theory to explain the peak structure found in mobility measurements and the depletion-field anomalies in the dynamical conductivity. The plasmon-mass minimum found in experiments is shown to be the result of the two scattering mechanisms. The mass increase at low density is due to reactive effects, but the mass increase at high density is due to dissipative effects. The increase and decrease of the cyclotron mass is explained by interaction effects and localization precursors, respectively, and is in good quantitative agreement with the experiment. Some comments are made for the cyclotron resonance in a frequency sweep. In the insulator phase a sharp resonance with variable cyclotron mass broadened by temperature effects is predicted.

I. INTRODUCTION

Two-dimensional electron systems in metal-oxide-semiconductors (MOS) structures are a widely used test system for transport in two dimensions.[1] Most relevant for the technical applications of these devices are the dc and ac conductivity.

In silicon systems two scattering mechanisms have been found to be most important.[1] Ionized-impurity scattering limits the mobility for low electron density, and the mobility increases with increasing electron density.[2] With increasing electron density the electrons of the two-dimensional layer are pushed to the Si/SiO_2 interface and the mobility decreases.[3] The interplay of these two scattering mechanisms gives a peak mobility at an intermediate electron density. Systematic work was done to get insight first into the parameters of the surface-roughness scattering[4] and second into the behavior of the peak mobility in dependence of the conditions of fabrication.[5] The density dependence of the mobility with both scattering mechanisms was calculated and compared with experiments by Matsumoto and Uemura,[6] who claimed that a third scattering mechanism is necessary to explain the experiments. More recent work on this subject was done in Ref. 7 in order to explain the mobility in experiments of Hartstein and Fowler, where Na ions have been drifted to the Si/SiO_2 interface.

The dynamical conductivity of silicon MOS systems exhibit some anomalies. At low electron density the dynamical conductivity has a maximum at finite frequency.[8] This behavior has been explained as localization[9] within the theory proposed by Götze[10] for the Anderson localization problem.[11] In Ref. 9 it was also found that with increased substrate bias the maximum of the conductivity decreases and goes to higher frequency.

It was shown that in strongly disordered systems the plasmon excitation energy is reduced with decreasing electron density,[12] in comparison with the free-electron result[1] (see also Ref. 13). Recently this behavior was interpreted in terms of a damped oscillator model.[14] A reduction of the plasmon energy was also found for increasing density[15] and interpreted as a mode-coupling effect.[16] A scaling behavior of the plasmon mass increase at low densities in different Si surfaces with Fermi energy was found.[17]

Cyclotron-resonance experiments exhibit some unexplained anomalies too.[1] With decreasing electron density the resonant magnetic field first increases and then decreases.[18] By drifting Na^+ ions to the interface, a strong reduction of the resonance field was found with increasing impurity concentration.[19] Strong anomalies in linewidth have been reported[20] as well as frequency anomalies in the line shape.[21] There is a long list of papers on this subject.[1] The decrease of the resonance field (decrease of the cyclotron mass) (Refs. 18 and 22) was explained by localization effects,[23] but a quantitative comparison with experiments was not possible. Among the various theories[24–27] to explain the anomalous mass, the memory-function approach of Ref. 28 was used and a mass increase was found theoretically.[29,30]

In a recent paper the influence of charged-impurity scattering on the static and dynamic transport properties of silicon MOS systems have been studied[31,32] within a multiple-scattering theory, originally proposed for the localization problem.[10] In Ref. 32 the influence of nonlinear screening behavior and the influence of impurities on the collective plasmon excitations have been studied in detail, extending some previous works on dynamical transport in two dimensions.[33,34] Anomalies found in measurements of the dynamical conductivity in a density sweep[35] have been explained by plasmon and localization anomalies.[36] Systematic work on the influence of impurity scattering and surface-roughness scattering on the mobility and the comparison with Na^+ drift experiments[37] has also been done within these multiple-scattering theories,[38] and good agreement between theory and experiment was found.

In the following we discuss the static and dynamic transport properties when both scattering mechanisms are present. The theory is used to explain measurements in connection with the peak mobility,[6] the substrate bias effects in the dynamical conductivity,[9] the plasmon mass minimum at a certain electron density,[17] and the cyclotron mass maximum[18] in Na^+-doped samples.[19]

The paper is organized as follows. In Sec. II we discuss our model and the essential equations to calculate the transport properties. In Sec. III static and dynamic aspects of the surface-roughness scattering are discussed. The interplay of ionized-impurity scattering and surface-roughness scattering is evaluated in Sec. IV, and the influence on the plasmon and cyclotron mass is studied in detail. In Sec. V a conclusion is given.

II. MODEL AND THEORY

A. Model

In this paper we calculate the transport properties of a two-dimensional interacting electron gas in the presence of charged-impurity scattering and surface-roughness scattering at temperature zero.

The Fourier transform of the interaction potential $V(\mathbf{q})$ for wave vector $\mathbf{q}$ is expressed as[2]

$$V(\mathbf{q})=\frac{2\pi e^2}{\epsilon_L}\frac{1}{q}F(q)\ , \tag{1a}$$

$$F(q)=\frac{1}{16}\left[1+\frac{\epsilon_{\rm in}}{\epsilon_{\rm sc}}\right]\frac{8+9q/b+3q^2/b^2}{(1+q/b)^3}+\frac{1}{2}\left[1-\frac{\epsilon_{\rm in}}{\epsilon_{\rm sc}}\right]\frac{1}{(1+q/b)^6}\ . \tag{1b}$$

e is the electron charge, $\epsilon_L=(\epsilon_{\rm in}+\epsilon_{\rm sc})/2$, $\epsilon_{\rm in}$ is the dielectric constant of the insulator, $\epsilon_{\rm sc}$ is the dielectric constant of the semiconductor, $1/b$ is the surface thickness of the electron gas given in Ref. 39, and $b^3=48\pi m_t e^2 N^*/\epsilon_{\rm sc}$ ($\hbar=1$ in this paper) with $N^*=\frac{11}{32}n+N_{\rm depl}$, where m_t is the electron mass perpendicular to the interface, $N_{\rm depl}$ is the depletion density, and n is the electron density. $F(q)$ is the form factor describing the finite extent of the wave function perpendicular to the interface.

We take into account two scattering mechanisms. The scattering by charged impurities located at the insulator-semiconductor interface is expressed by the random potential $\langle\,|\,U_1(\mathbf{q})\,|\,\rangle^2$,

$$\langle\,|\,U_1(\mathbf{q})\,|^2\rangle=n_i\left[\frac{2\pi e^2}{\epsilon_L}\frac{1}{q}F_i(q)\right]^2\ , \tag{2a}$$

$$F_i(q)=\frac{1}{(1+q/b)^3}\ . \tag{2b}$$

$F_i(q)$ is a form factor for the finite extent of the wave function,[2] n_i is the density of scatterers. The scattering by uncharged impurities via a random potential $\langle\,|\,U_2(\mathbf{q})\,|^2\rangle$ is characterized by the two length parameters of the surface roughness scattering Δ and Λ and we use[40]

$$\langle\,|\,U_2(\mathbf{q})\,|^2\rangle=\pi\Delta^2\Lambda^2[\Gamma(\mathbf{q})]^2e^{-q^2\Lambda^2/4}\ , \tag{3a}$$

$$\Gamma(\mathbf{q})=\gamma(\mathbf{q})+\gamma_i(\mathbf{q})\ , \tag{3b}$$

$$\gamma(\mathbf{q})=q_s\epsilon_F\left\{\left[1+\frac{2N_{\rm depl}}{n}\right]-\frac{2\epsilon_L}{\epsilon_{\rm sc}}\bar{\epsilon}\left[\left[1+\frac{N_{\rm depl}}{n}\right]\left[1-\frac{1}{(1-q/b)^3}\right]-\frac{1}{2}\left[1-\frac{1}{(1-q/b)^6}\right]\right]\right\}\ . \tag{3c}$$

q_s is the Thomas-Fermi screening vector, ϵ_F the Fermi energy related to the density $n=(g_v/\pi)m\epsilon_F$, m is the mass of the electron in the two-dimensional plane, g_v is the valley degeneracy factor, spin degeneracy is already included, and

$$\bar{\epsilon}=\left[1-\frac{\epsilon_{\rm in}}{\epsilon_{\rm sc}}\right]\Big/\left[1+\frac{\epsilon_{\rm in}}{\epsilon_{\rm sc}}\right]\ .$$

$\gamma_i(\mathbf{q})$ gives only small effects to $\Gamma(\mathbf{q})$ and will not be given here.[41] Λ characterizes the length of the potential fluctuations and Δ the height. The asymptotic values of $\gamma(\mathbf{q})$ are given as

$$\gamma(\mathbf{q})=2\pi e^2(n+2N_{\rm depl})\times\begin{cases}\dfrac{1}{\epsilon_L}, & q\to 0\\ \dfrac{1}{\epsilon_{\rm sc}}, & q\to\infty\end{cases} \tag{4}$$

and the result for $q\to\infty$ was used before.[6] For both scattering mechanisms the random potential is approximated as

$$\langle\,|\,U(\mathbf{q})\,|^2\rangle=\langle\,|\,U_1(\mathbf{q})\,|^2\rangle+\langle\,|\,U_2(\mathbf{q})\,|^2\rangle\ . \tag{5}$$

In the following we evaluate the conductivity for Si(100) MOS systems and use, as parameters, $\epsilon_{\rm sc}=11.5$, $\epsilon_{\rm in}=3.9$, $m_t=0.916m_0$, $m=0.19m_0$, and $g_v=2$. m_0 is the vacuum mass of the electron.

B. Theory

For the calculation of the transport properties we use the self-consistent current relaxation theory of Ref. 10, generalized to an interacting electron gas.[31,32] In this memory-function approach the conductivity $\sigma(z)$ is expressed in a generalized Drude form with z as the complex frequency via[28]

$$\sigma(z)=\frac{ne^2}{m}\frac{i}{z+M(z)}\ . \tag{6}$$

$M(z)$ is the frequency-dependent current relaxation kernel with real (reactive) and imaginary (dissipative) parts: $M(z=\omega\pm i0)=M'(\omega)\pm iM''(\omega)$.

With a mode-coupling approximation $M(z)$ is given in a generalized Fermi golden rule[10] as

$$M(z)=\frac{1}{dnm}\sum_{\mathbf{q}} q^2\langle\,|\,U(\mathbf{q})\,|\,^2\rangle\phi(\mathbf{q},z)\ . \tag{7}$$

d is the dimension of the system and $\phi(\mathbf{q},z)$ is the density relaxation function for wave vector $\mathbf{q}$ and complex frequency z. $\phi(\mathbf{q},z)$ is given as[31]

$$\phi(\mathbf{q},z)=\frac{\phi^R(\mathbf{q},z+M(z))}{1+M(z)\phi^R(\mathbf{q},z+M(z))/g^J(\mathbf{q})}\ , \tag{8}$$

and $\phi^R(\mathbf{q},z)$ is the density relaxation function of the system without impurities. $g^J(\mathbf{q})$ is the compressibility of the system. By assuming that the impurities do not change $g^J(\mathbf{q})$ drastically, we replace $g^J(\mathbf{q})$ by the compressibility of the system without impurities, $g^R(\mathbf{q})$. The model of the electron gas without impurities consists then of the free-gas part and the Coulomb part.

In the random-phase approximation with local-field corrections $G(\mathbf{q})$,[42] $\phi^R(\mathbf{q},z)$ is expressed in terms of the free-gas relaxation function and the free-gas compressibility $g^0(\mathbf{q})$:

$$\phi^R(\mathbf{q},z)=\left[\frac{g^R(\mathbf{q})}{g^0(\mathbf{q})}\right]^2 \times\frac{\phi^0(\mathbf{q},z)}{1+g^R(\mathbf{q})/g^0(\mathbf{q})[1-G(\mathbf{q})]V(\mathbf{q})z\phi^0(\mathbf{q},z)}\ , \tag{9a}$$

$$g^R(\mathbf{q})=\frac{g^0(\mathbf{q})}{1+V(\mathbf{q})[1-G(\mathbf{q})]g^0(\mathbf{q})}\ . \tag{9b}$$

The connection between $\phi^0(\mathbf{q},z)$ and the Lindhard formula[13] for the susceptibility $\chi^0(\mathbf{q},z)$ is given by

$$\phi^0(\mathbf{q},z)=\frac{1}{z}[\chi^0(\mathbf{q},z)-g^0(\mathbf{q})]\ .$$

For $G(\mathbf{q})$ we use the Hubbard form[43]

$$G(\mathbf{q})=\frac{1}{2g_v}\frac{q}{(q^2+k_F^2)^{1/2}}\ ,$$

with k_F as Fermi momentum.

Equations (5) and (7)–(9) are a closed nonlinear system of equations for calculating $\phi(\mathbf{q},z)$ and $M(z)$. It can be solved iteratively.[44,45] When $\phi^R(\mathbf{q},z)$ and $g^R(\mathbf{q})$ are replaced by $\phi^0(\mathbf{q},z)$ and $g^0(\mathbf{q})$, the equations have been discussed before,[10,44,45] and they describe a transition from a metal with finite dc conductivity to an insulator with finite dc polarizability $X(z=0)$.[10] For $\langle\,|\,U_2(\mathbf{q})\,|\,^2\rangle=0$ the equations have been discussed recently.[31,32,36] For $z=0$ the equations have also been solved numerically in connection with the peak mobility.[38] For $z=0$, $G=0$, and $\langle\,|\,U_1(\mathbf{q})\,|\,^2\rangle=0$ or $\langle\,|\,U_2(\mathbf{q})\,|\,^2\rangle=0$, the equations are identical to the one discussed in Ref. 40 or 2, respectively, when self-consistent effects of the theory are neglected. For a more complete discussion of the approximations of the theory and the derivation of the fundamental equations, see Ref. 32.

III. SURFACE-ROUGHNESS SCATTERING

In the following we solve our self-consistent equations for $\langle\,|\,U_1(\mathbf{q})\,|\,^2\rangle=0$. Then the conductivity is only limited by the surface-roughness scattering first mentioned in Ref. 46.

A. Mobility

With increasing N_{depl} or n the electrons are pushed to the Si/SiO_2 interface, the surface-roughness scattering increases, and the mobility $\mu=\sigma/ne$ decreases. In Fig. 1 we compare our result for the mobility as function of density with the approximations $\gamma_i(\mathbf{q})=0$ and $G=0$. Because local-field corrections decrease the screening properties of the electron gas, the mobility is higher when local-field corrections are neglected. This effect for low density is greater than the $\gamma_i(\mathbf{q})$ effect in Eq. (3b) [$\gamma_i(\mathbf{q})$ gives the contribution of the image potential[40]]; see Fig. 1. From the potential function [Eq. (3a)] one would expect that $\mu\propto 1/(\Delta\Lambda)^2$. In Fig. 2 we have shown that, for fixed $(\Delta\Lambda)$, derivations for increasing electron densities rise because of the fluctuation cutoff in Eq. (3a) when $k_F^2>1/\Lambda^2$. For $n>n_{\text{LR}}=1/(\pi\Lambda^2)$ the backscattering of the electrons is suppressed, the random potential becomes long ranged,[45] and the mobility decreases as $\mu\propto 1/\sqrt{n}$ for $n\gg n_{\text{LR}}$.

There is not very much known about the parameters Δ

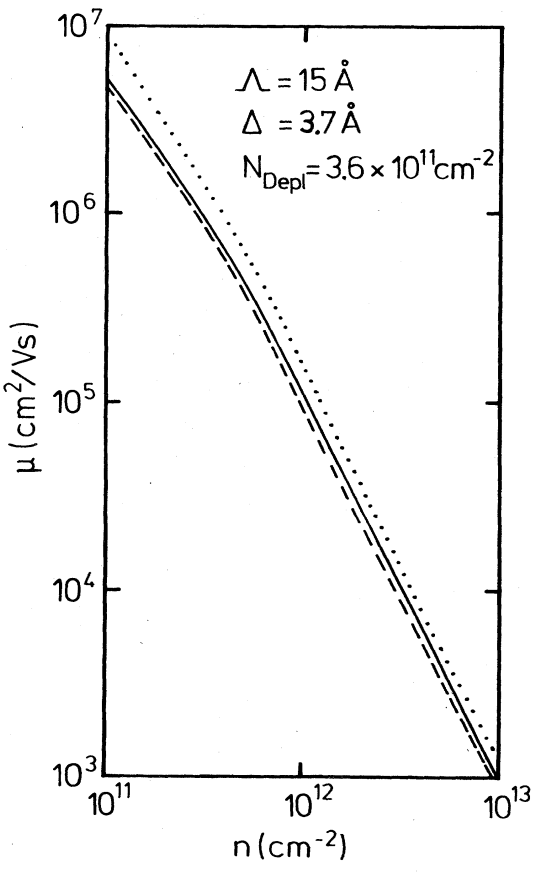

FIG. 1. Mobility versus density for surface-roughness scattering. The solid line is for $\Gamma=\gamma+\gamma_i$ and $G\neq 0$. The dashed and dotted lines are for $\Gamma=\gamma$, $G\neq 0$ and $\Gamma=\gamma+\gamma_i$, $G=0$, respectively.

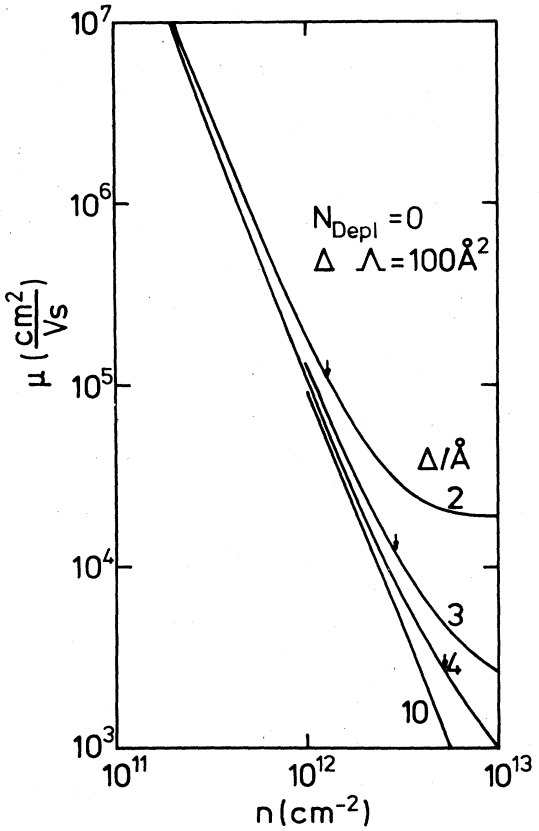

FIG. 2. Mobility versus density for surface-roughness scattering for various values of Δ. The arrows indicate $n_{LR}=(1/\pi)(1/\Lambda^2)$.

and Λ for the surface-roughness scattering. For a long time it was assumed that Λ=15 Å and Δ=3.7 Å should be most realistic.[1] It was especially argued[1] that because of the above-mentioned suppression of backscattering for high n, Λ has to be smaller than about 15 Å. However, recently, also values of Λ of about 30 Å have been used to explain experiments.[47–49] High-resolution transmission-electron-microscopy (TEM) micrographs have been made to determine the parameters microscopically, and Δ=2 Å and Λ=40 Å have been found.[50] The influence of annealing conditions on the mobility and the surface roughness have been studied by Hahn and Henzler,[51] and a strong correlation between Hall mobilities and atomic roughness was reported. thus, our Λ values between 50 and 10 Å, chosen in Fig. 2, seem to be realistic, and the effect of backscattering suppression should be measurable.

B. Dynamic aspects

In Fig. 3 the imaginary part of the relaxation function, normalized to n^2, is shown as a function of frequency for various densities. The dc value demonstrates that the $\mu(n)$ dependence is weaker than $1/n^2$, and the frequency dependence demonstrates that with increasing density the frequency dependence becomes weaker. But for $n=1\times10^{12}$ cm^{-2} there exists a strong increase of the relaxation rate, as in the case of charged-impurity scattering.[32]

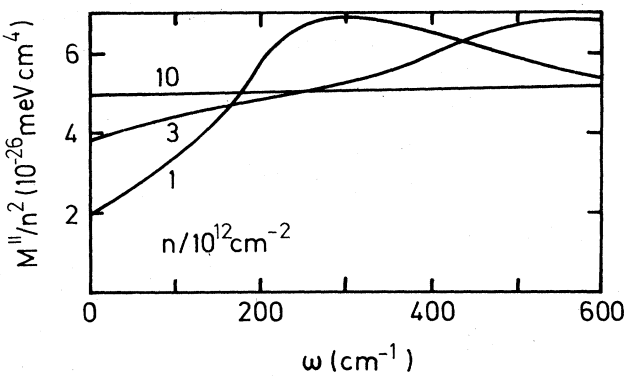

FIG. 3. Relaxation rate normalized to density squared as function of frequency for surface-roughness scattering. The parameters are Λ=15 Å, Δ=3.7 Å, and $N_{depl}=0$.

When self-consistent effects are ignored in our theory by setting $M(z)=0$ in Eq. (8), we receive the zero-order result $M_0(z)$ of our theory. $M_0''(\omega)$ can be written as[32] (where the $\mathbf{q}$ summation is performed only over the particle-hole spectrum)

$$M_0''(\omega)=\frac{1}{2nm}\sum_{\mathbf{q}} q^2\langle\,|\,U_{scr}(\mathbf{q})\,|\,^2\rangle \times R(\mathbf{q},\omega)\phi^{0\prime\prime}(\mathbf{q},\omega)+M_{0p}''(\omega)\,, \tag{10a}$$

$$\langle\,|\,U_{scr}(\mathbf{q})\,|\,^2\rangle=\frac{\langle\,|\,U(\mathbf{q})\,|\,^2\rangle}{\{1+V(\mathbf{q})[1-G(\mathbf{q})]g^0(\mathbf{q})\}^2}\,, \tag{10b}$$

$$R(\mathbf{q},\omega)=\left|\frac{1+V(\mathbf{q})[1-G(\mathbf{q})]g^0(\mathbf{q})}{1+V(\mathbf{q})[1-G(\mathbf{q})]\chi^0(\mathbf{q},\omega)}\right|^2. \tag{10c}$$

$\langle\,|\,U_{scr}(\mathbf{q})\,|\,^2\rangle$ is the statical screened random potential and $\chi^0(\mathbf{q},\omega)$ is the Lindhard function.[13] $M_{0p}''(\omega)$ is the contribution of the plasmon decay channel. In an interacting electron gas the current can decay into electron-hole excitations, which is the first part on the right-hand side of Eq. (10a), and into plasmons, which is the second part on the right-hand side of Eq. (10a). For $\langle\,|\,U(\mathbf{q})\,|\,^2\rangle\propto q^{2\alpha}$, we get

$$M_{0p}''(\omega)\sim|\,\omega\,|^{9+4\alpha}\ \text{as}\ \omega\to0\,. \tag{11}$$

For the surface-roughness scattering with $\alpha=0$, we obtain

$$M_{0p}''(\omega\to0)=C\epsilon_F(\omega/\epsilon_F)^9\,, \tag{12a}$$

$$C=\frac{\pi}{4^8}(\Delta q_s)^2(\Lambda q_s)^2\left[\frac{2k_F}{q_s}\right]^8\left[1+2\frac{N_{depl}}{n}\right]^2. \tag{12b}$$

The various contributions to the relaxation rate are shown in Fig. 4. The difference between the dashed line and the solid line is the plasmon decay channel. The dotted line represents a noninteracting electron gas with a static screened electron impurity interaction. The difference between the dashed line and the dotted line is due to the dynamical breakdown of screening. We want to men-

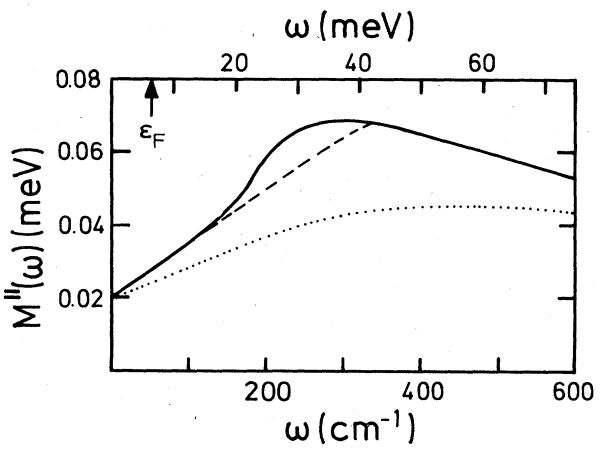

FIG. 4. Relaxation rate as function of frequency for surface-roughness scattering according to Eq. (10). The solid line is for $M''_{0p}(\omega)\neq 0$ and $R(\mathbf{q},\omega)$ after Eq. (10c). The dashed and dotted lines are for $M''_{0p}(\omega)=0$ and $R(\mathbf{q},\omega)$ after Eq. (10c) and $R(\mathbf{q},\omega)=1$, respectively. For all lines we used $n=1\times 10^{12}$ cm^{-2}, $\Delta=15$ Å, $\Lambda=3.7$ Å, and $N_{\text{depl}}=0$.

tion that in Figs. 1—4 only percent effects exist between the zero-order result and the self-consistent theory. In Ref. 32 the condition for the metal-insulator transition was given by the parameter A, depending on $\langle |U(\mathbf{q})|^2\rangle$ and $g_R(\mathbf{q})$, to be one. For surface-roughness scattering alone, with the parameter of Figs. 1—4, this parameter A is very small. This is why self-consistency effects can be neglected.

IV. IMPURITY AND SURFACE-ROUGHNESS SCATTERING

In this section both scattering mechanisms are taken into account.

A. Peak mobility

In this subsection we give additional results for the mobility, as discussed before in Ref. 38.

The characteristic density dependence of the mobility in silicon MOS systems consists of the increasing mobility at low density due to charged-impurity scattering and a decreasing mobility at high density due to surface-roughness scattering. The corresponding peak mobility μ_m at a characteristic density n_m depends on the parameters n_i, N_{depl}, Δ, and Λ. For $n_i=3\times 10^{11}$ cm^{-2} the mobility versus density is shown in Fig. 5. For low density the theory describes a transition to an insulator phase[31,32] and the mobility decreases to zero at the mobility edge. As already mentioned, the surface roughness gives only small effects to the phase-transition point, and the low-density regime is not influenced by the surface-roughness parameters. A finite depletion density increases the insulator phase and increases the surface-roughness scattering. Thus, for finite N_{depl} the mobility is decreased for all densities; see Fig. 5(c). As far as backscattering is possible in the surface-roughness channel, a peak structure in the

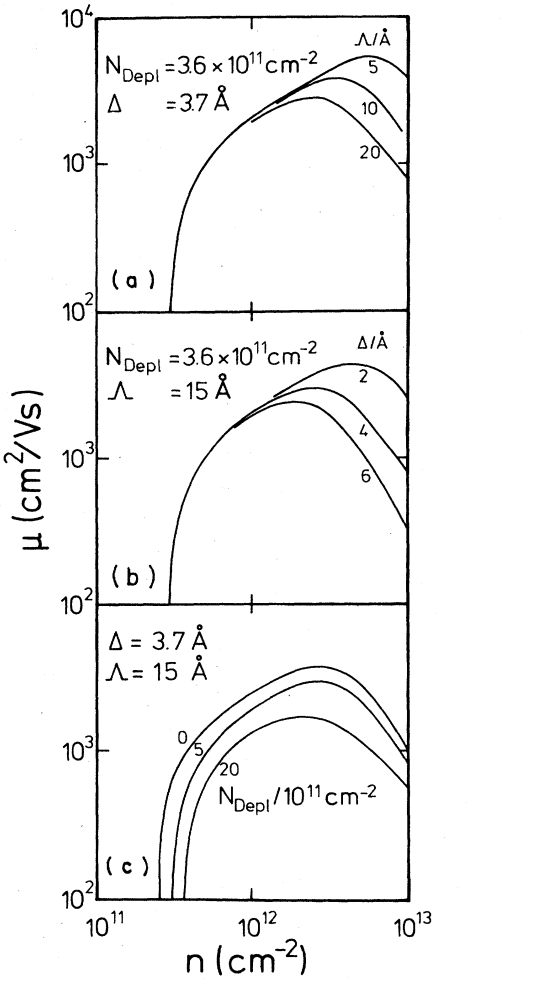

FIG. 5. Mobility versus density for $n_i=3\times 10^{11}$ cm^{-2} and (a) different values of Λ, (b) different values of Δ, and (c) different values of N_{depl}.

conductivity-versus-density curves also exists, Fig. 6, but the peak in the conductivity is at higher density than the peak in the mobility; for comparison, see Fig. 5(c). Depending on the parameters, the peak may be at such a high density that the second subband, which is neglected here, is already occupied, and then our theory fails.

The mobility versus density in comparison with experiments is shown in Fig. 7, together with the zero-order result of our theory. This experiment has already been discussed before within our theory, but a simplified vertex for the surface-roughness scattering has been used.[32] Only two scattering mechanisms are sufficient to explain the data, in contradiction to Ref. 6, where three mechanisms have been used. Due to localization at low density the peak structure in the mobility is strongly enhanced in comparison with our zero-order result, the dotted line in Fig. 7. Notice that for $n<2\times 10^{11}$ cm^{-2} the theory predicts a strong suppression of the mobility. Unfortunately, no data are available in this regime. Notice also that self-consistency effects are relevant for $n<2n_m$. Thus the peak structure is in a density range where nonlinear behavior must be taken into account.

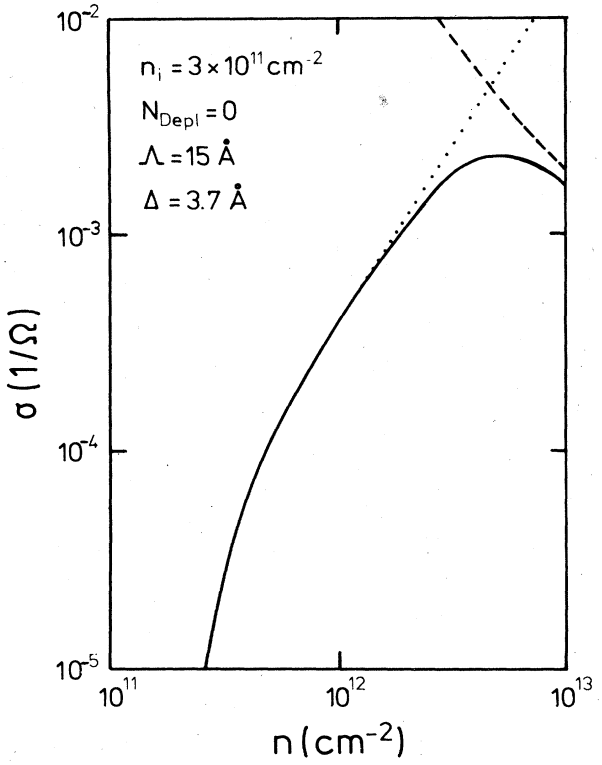

FIG. 6. Conductivity versus density. Solid line for impurity and surface-roughness scattering, dashed line for surface-roughness scattering, and dotted line for impurity scattering.

Let us make some statements about the impurity scattering. The density dependence of the impurity scattering at low density in the zero-order result comes from the density dependence of the structure factors $F(q)$ and $F_i(q)$; see also Fig. 1 in Ref. 32. Thus the normally used statement that mobility increases because of screening is incorrect. The existence of a mobility edge is the real reason for the strong density dependence of the mobility at low density.

In Ref. 38 μ_m versus n_m for fixed N_{depl}, Δ, and Λ was shown as function of n_i. The experimental finding[37] of decreasing μ_m and increasing n_m with increasing Na^+ contamination was explained quantitatively. The μ_m-versus-n_m dependence for various chosen parameters of the surface-roughness scattering and N_{depl} is shown in Fig. 8(a) and should be compared with Fig. 8(b), where some experimental results[9,21,37,52,53] are shown. The lines in Fig. 8(a) for given Δ, Λ, and N_{depl} have as an implicit parameter the impurity density. With increasing impurity density, μ_m decreases and n_m increases. For large n, backscattering is suppressed and no maximum in the mobility is found. The dots in Fig. 8(b) are measured by a

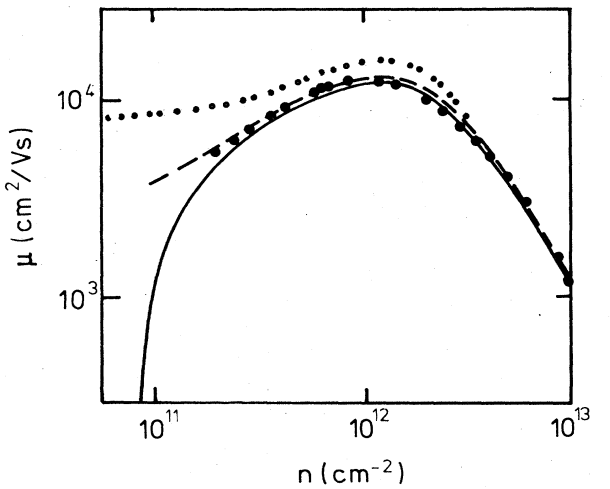

FIG. 7. Mobility versus density according to our theory as solid curve with $n_i = 0.55\times10^{11}$ cm^{-2}, $N_{\text{depl}} = 3.6\times10^{11}$ cm^{-2}, $\Lambda = 15$ Å, and $\Delta = 3.7$ Å. The dotted line is our zero-order result. The dashed curve denotes the theoretical result of Ref. 6. The dots are the experimental results of Kawaji (Ref. 6).

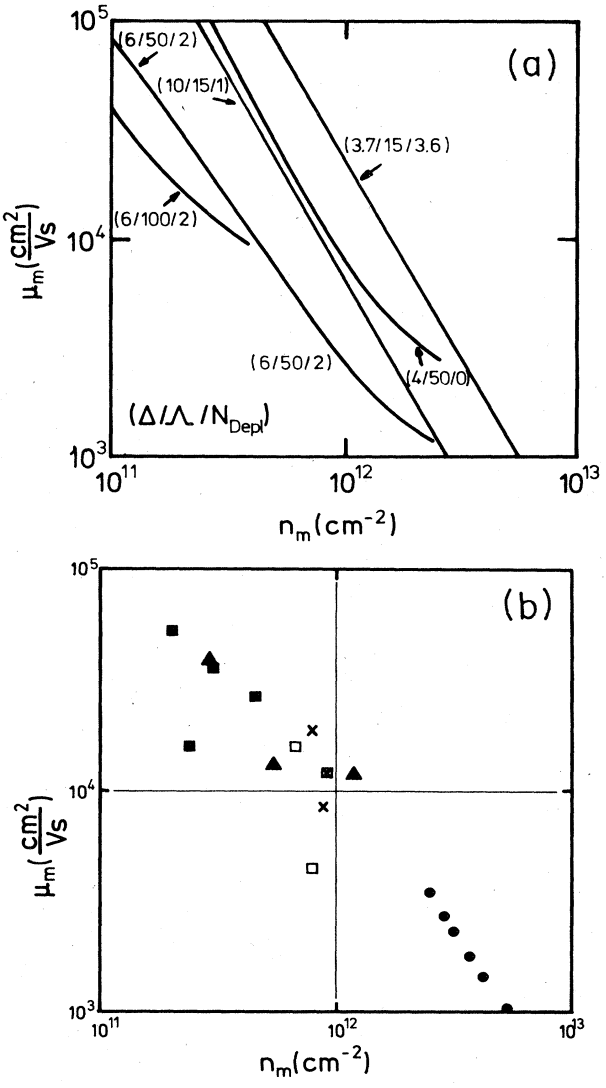

FIG. 8. (a) Peak mobility versus peak density according to our theory for various values of Δ, Λ, and N_{depl}. (b) Peak mobility versus peak density from the experiment. Solid squares are due to Ref. 52, open squares after Ref. 9, triangles after Ref. 53, crosses after Ref. 21, and dots after Ref. 37.

systematic increase of Na scatterers in one sample[37] with fixed surface-roughness scattering and are in good agreement with the line for $\Delta=3.7$ Å, $\Lambda=15$ Å, and $N_{\text{depl}}=3.6\times10^{11}$ cm^{-2}.[38] Samples with high peak mobility[52,53] seem to have higher values of Λ than the samples with lower peak mobility; compare Fig. 8(a) with Fig. 8(b). More systematic measurements of the mobility would be useful to get some insight into the parameters of the surface-roughness scattering.

B. Dynamical conductivity

The dynamical conductivity can be measured in a density sweep at finite laser frequency.[35,36] In Figs. 9(a) and 9(b) a representative example is shown for the behavior of M'' and M' curves for various frequencies. As a function of density there are two extremal values in the M''-versus-density curves. The one at higher density is the one which comes from the interplay between impurity scattering and surface-roughness scattering and is a reflection of the peak mobility. The one at lower density comes from the interaction effects and corresponds to the maximum in $M''(\omega)$ as a function of ω; see Fig. 3 and Ref. 32. For low frequencies and low density, self-consistency effects are important; this is not the case for high frequencies. At high density the relaxation rate at finite frequency is higher than the static one. This effect was measured in cyclotron-resonance experiments; see Fig. 9 of Ref. 22. Via Kramers-Kronig relations the frequency dependence of $M''(\omega)$ is transferred to a frequency dependence of

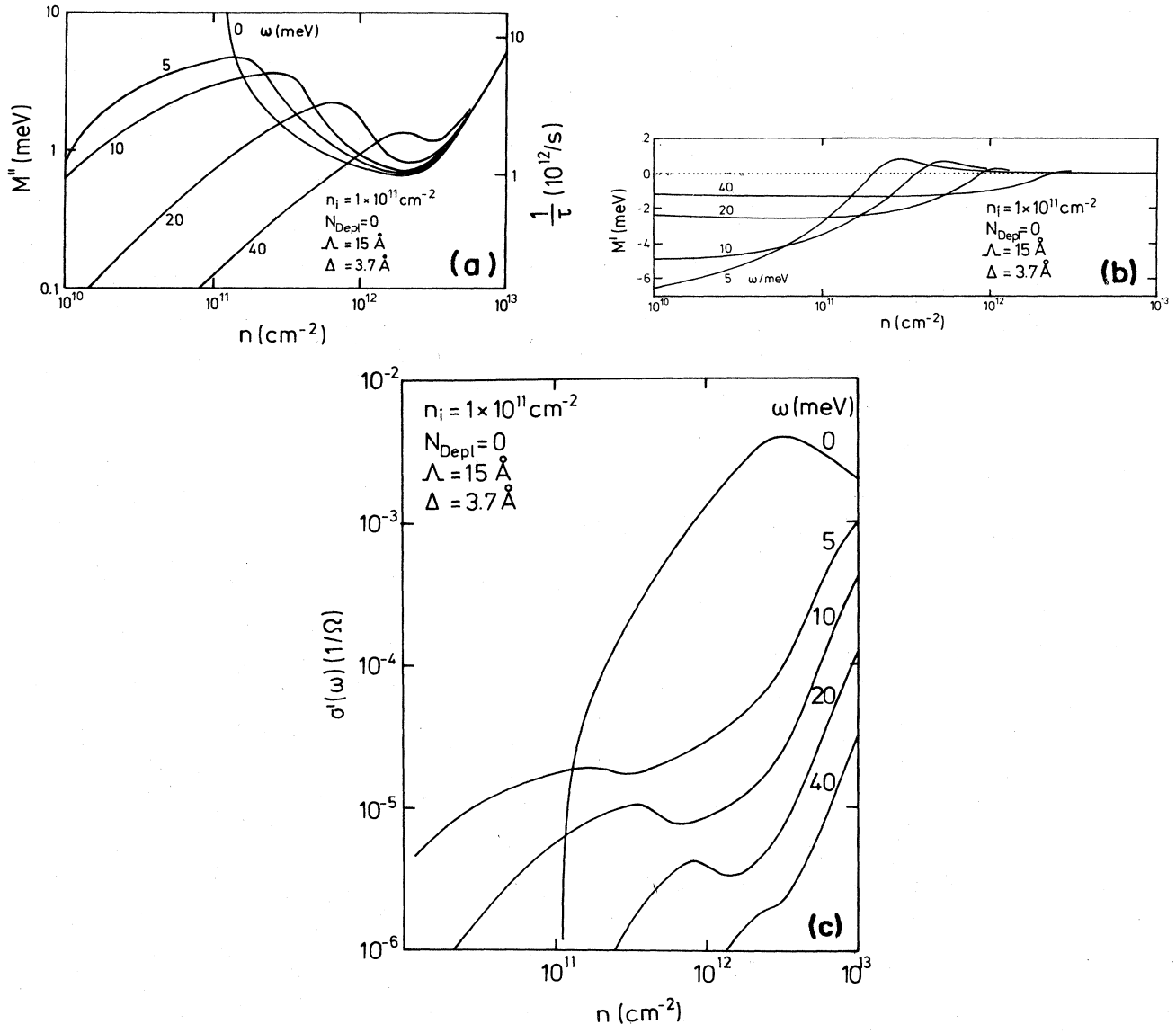

FIG. 9. (a) Dissipative part of the relaxation kernel as a function of density for various frequencies. (b) Reactive part of the relaxation kernel as a function of density for various frequencies. (c) Dynamical conductivity as a function of density for various frequencies.

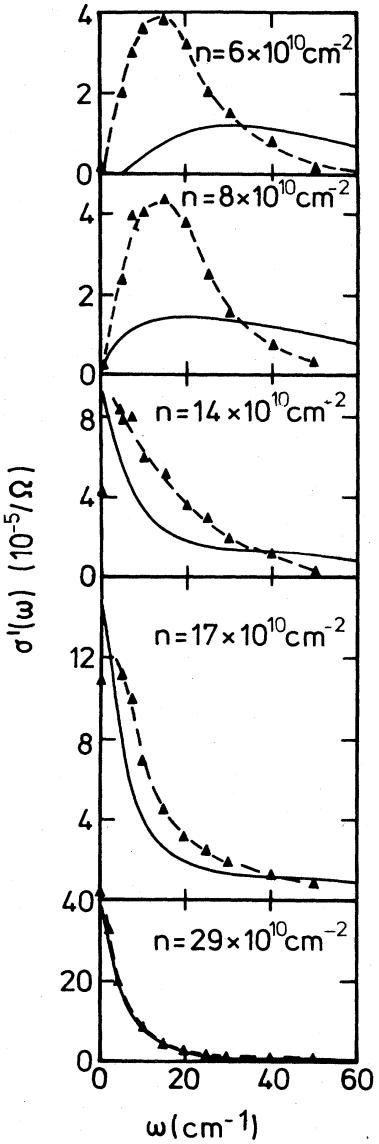

FIG. 10. Dynamical conductivity versus frequency according to our theory for various densities and $n_i=4.5\times10^{10}$ cm^{-2}, $N_{\text{depl}}=4.2\times10^{11}$ cm^{-2}, $\Lambda=15$ Å, and $\Delta=3.7$ Å. The dashed lines with the triangles are experimental results (Ref. 9).

$M'(\omega)$. For increasing $M''(\omega)$ with frequency, $M'(\omega)$ increases and is positive; see Fig. 9(b) for high density. For low density $M''(\omega)$ decreases with increasing frequency, and $M'(\omega)$ also decreases, and $M'(\omega)$ is negative. Thus there exists a frequency for fixed density, where $M'(\omega)$ changes sign. For fixed frequency there exists a density where M' changes sign. This is an interaction effect due to the maximum in $M''(\omega)$ which comes from the dynamics of plasmons and from dynamical screening breakdown. This physics is already included in the zero-order result of our theory when self-consistency effects are neglected. Self-consistency effects decrease the frequency (for fixed density) and increase the density (for fixed frequency) where M' changes sign. Later we will see that $M'(n,\omega)$ determines some dynamical experiments. The point where M' changes sign is especially important for some experiments (see Fig. 17). This is the reason why a nonlinear theory is important for a correct interpretation of the experiments. In Fig. 9(c) the dynamical conductivity is shown as a function of frequency. For $\omega=0$ a peak conductivity exists, and for finite frequency a peak structure[35] due to plasmon dynamics[36] can be seen. This peak structure is only visible in a finite-frequency range.

In Ref. 32 it was shown that the theory can explain many experiments; see also Ref. 54 for subband physics. In Fig. 10 we demonstrate that the experiment by Allen, Wilson, and Tsui[9] cannot be explained by charged-impurity scattering. For low density considerable deviations between theory and experiment exist. The reason for the discrepancies are not clear for us. Perhaps an additional scattering mechanism must be introduced; for example, neutral-impurity scattering seems to be a realistic candidate. The two upper figures show curves for an insulating phase with zero dc conductivity and a maximum at finite frequency. The curves with $n=1.4\times10^{11}$ and 1.7×10^{11} cm^{-2} exhibit strong frequency anomalies due to interaction and localization effects, and the maximum of the conductivity is at zero frequency.

In Fig. 11 the dynamical conductivity in the localized phase is shown as function of frequency with N_{depl} as a parameter. With increasing N_{depl} the maximum of the conductivity decreases and the maximum goes to higher frequencies. Such behavior has been found by applying a substrate bias on the sample (see Fig. 5 of Ref. 9). Our theory predicts that with increased N_{depl} the insulator phase increases[32]—see Fig. 5(c)—and thus the trend of the experiment is understandable. This effect also happens when some additional scattering mechanism due to neutral impurities[55] is present. Unfortunately, see Fig. 10, the conductivity scala and the frequency scala of the experiments cannot be explained by charged-impurity scattering.

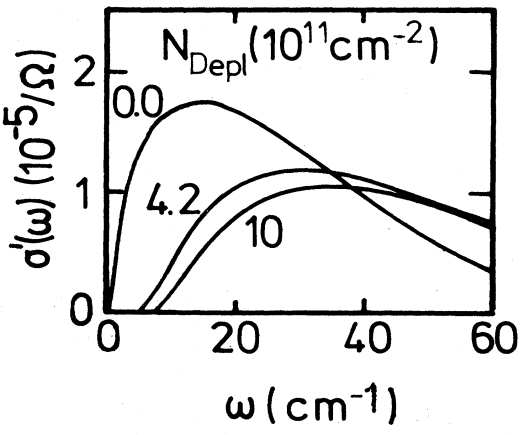

FIG. 11. Dynamical conductivity as function of frequency for various N_{depl} and $n_i=4.5\times10^{10}$ cm^{-2}, $n=6\times10^{10}$ cm^{-2}, $\Lambda=15$ Å, and $\Delta=3.7$ Å.

C. Resonance anomalies

In a recent paper the anomalies of charged-impurity scattering on the collective plasmon excitations have been discussed.[32] The hydrodynamic density propagator can be expressed as

$$\phi''(\mathbf{q},\omega)=g^R(\mathbf{q})\omega_{p0}^2(q) \times \frac{M''(\omega)}{[\omega^2+\omega M'(\omega)-\omega_{p0}^2(q)]^2+\omega^2 M''(\omega)^2} , \quad (13a)$$

and

$$\omega_{p0}^2(q)=\frac{2\pi}{\epsilon_L}\frac{ne^2}{m}q$$

is the classical plasmon dispersion relation in two dimensions. For $\omega \gg |M(z)|$ we get, for the energy of the plasmons Ω and for the half-width at half maximum (HWHM) of the density propagator Γ_p,[32]

$$\Omega=\omega_{p0}-M'(\omega_{p0})/2 . \quad (13b)$$

$$\Gamma_p=M''(\omega_{p0})/2 . \quad (13c)$$

When reactive effects are neglected, $M'=0$, we get

$$\Omega=\omega_{p0}[1-\beta(M''(\omega_{p0})/\omega_{p0})^2]^{1/2} , \quad (13d)$$

with $\beta=\frac{1}{2}$ instead of the value $\beta=\frac{1}{4}$ given before.[14]

For the subband physics with subband distance ϵ_{10}, the Ando formula[56] for the transverse conductivity $\sigma_\perp'$ has been generalized[54] to

$$\sigma_\perp'(\omega)=\frac{ne^2}{m_t}\frac{2\omega^2 M_\perp''(\omega)}{[\omega^2+2\omega M_\perp'(\omega)-\epsilon_{10}^2]^2+4\omega^2 M_\perp''(\omega)^2} , \quad (14a)$$

and $M_\perp(z)$ is the transverse current relaxation kernel. For $\omega \gg |M_\perp(z)|$ we obtain, for the disorder-induced subband energy ω_{sb}, with linewidth Γ_{sb} (HWHM),[54]

$$\omega_{sb}=\epsilon_{10}-M_\perp'(\epsilon_{10}) , \quad (14b)$$

$$\Gamma_{sb}=M_\perp''(\epsilon_{10}) . \quad (14c)$$

For the cyclotron-resonance experiments we use[24]

$$\sigma(z)=\frac{1}{2}\frac{ne^2}{m}\left[\frac{i}{z+\omega_B+M_B(z)}+\frac{i}{z-\omega_B+M_B(z)}\right] , \quad (15a)$$

and $\omega_B=eB/m$ is the cyclotron frequency. $M_B(z)$ is the current relaxation kernel in the presence of a magnetic field B. The resonance in a B sweep is found, for $|\omega \gg |M_B(z)|$, at the magnetic field $B_R=m\omega_R/e$ with linewidth Γ_R (HWHM),[24]

$$\omega_R=\omega+M_B'(\omega) , \quad (15b)$$

$$\Gamma_R=M_B''(\omega) . \quad (15c)$$

From the formulas (13)–(15) the relevance of a generalized Drude relaxation rate can be seen. The shift of the resonance is always determined by $M'(\omega)$ instead of the shift of a damped oscillator, given by M''.[2] When approximations are available for $M(z)$, $M_\perp(z)$, and $M_B(z)$, a real test of the theory is possible. For the subband physics we made the approximation $M_\perp(z)=\frac{1}{2}M(z)$, neglecting scattering processes in the upper subband.[54] For the cyclotron resonance we use in the following $M_B(z)=M(z)$,[29,30] and the results will be discussed later in this paper. The relevance of Figs. 9(a) and 9(b) is demonstrated in Eqs. (13)–(15).

D. Plasmon anomalies

Charged-impurity scattering shifts the plasmon energy to lower frequency.[33] First for higher density because of positive $M'(\omega)$ [see Eq. (13)], and later for lower-density, dissipative effects become dominant in comparison with $M'(\omega)$.[32] Before the mobility edge is reached, the plasmon mode is overdamped due to dissipative effects (see Fig. 16 of Ref. 32). The shift can be interpreted as an effective plasmon mass m_p different from the conductivity mass m by

$$m_p=m\left[\frac{\omega_{p0}}{\Omega}\right]^2 . \quad (16)$$

In Fig. 12 we have shown m_p/m_0 as a function of density for $q=1.256\times10^5$ cm^{-1} and for various values of the surface-roughness parameter Δ. Also shown is the damping parameter of the plasmons $M''(\Omega)/\Omega=1/[\tau(\Omega)\Omega]$ and $\tau(\Omega)$ is the relaxation time of the plasmons. Only for $M''/\Omega \ll 1$ are the plasmons well de-

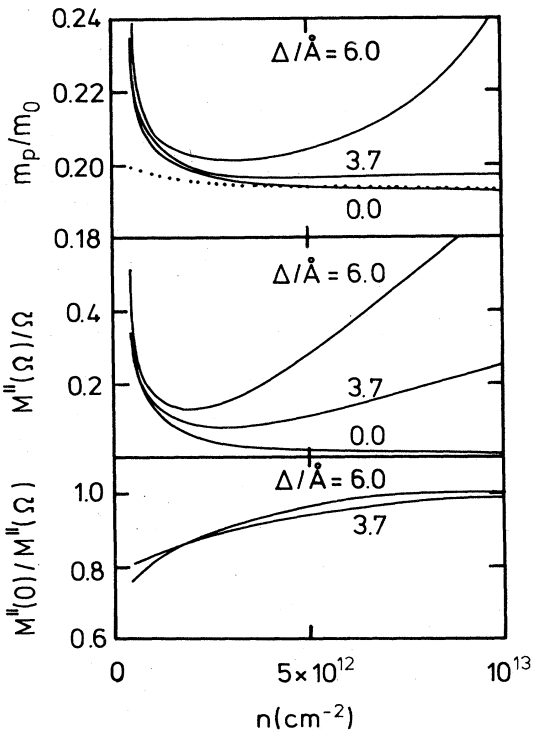

FIG. 12. Plasmon mass, dissipative relaxation kernel normalized to plasmon frequency, and $M''(0)/M''(\Omega)$ as a function of density according to our theory for various values of Δ and $q=1.256\times10^5$ cm^{-1}. The parameters of the theory are $n_i=1\times10^{11}$ cm^{-2}, $N_{depl}=3.6\times10^{11}$ cm^{-2}, and $\Lambda=15$ Å. For the dotted line, see text.

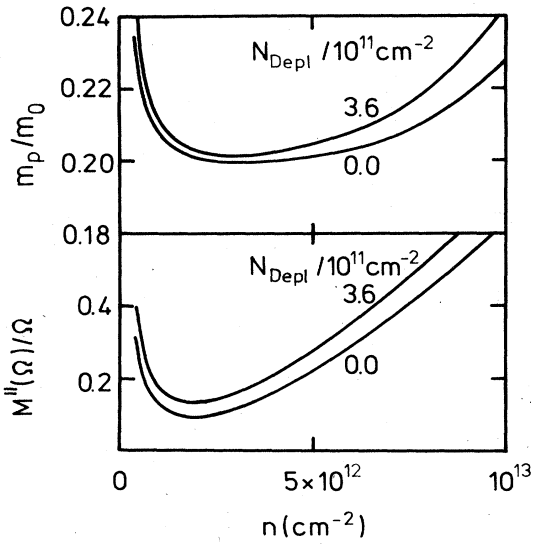

FIG. 13. Plasmon mass and dissipative relaxation kernel normalized to plasmon frequency as function of density for $N_{\rm depl}=0$ and $N_{\rm depl}=3.6\times10^{11}$ cm^{-2}. The other parameters of the theory are $n_i=1\times10^{11}$ cm^{-2}, $\Lambda=15$ Å, $\Delta=6$ Å, and $q=1.256\times10^{5}$ cm^{-1}.

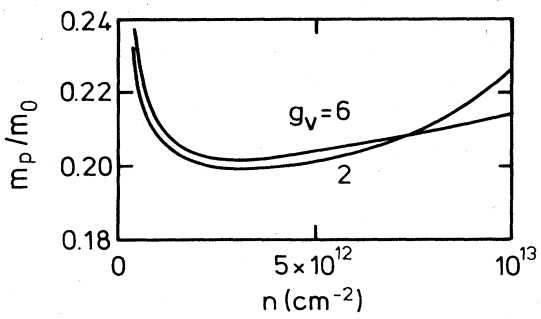

FIG. 14. Plasmon mass versus density for $g_v=2$ and $g_v=6$. The other parameters of the theory are $n_i=1\times10^{11}$ cm^{-2}, $\Lambda=15$ Å, $\Delta=6$ Å, $q=1.256\times10^{11}$ cm^{-2}, and $N_{\rm depl}=0$.

fined in the relaxation spectrum $\phi''(\mathbf{q},\omega)$ [see Eq. (13a)]. Ω was determined as the maximal value in $\phi''(\mathbf{q},\omega)$. The dotted line in Fig. 12 gives the q corrections due to $G(q)$, $F(q)$, and higher terms in a hydrodynamic expansion[13] to the classical dispersion relation, asymptotically expressed as

$$\omega_p^2=\omega_{p0}^2\left[1-\frac{1}{2g_v}\frac{q}{k_F}+\tilde{F}(q)+\frac{3}{4}\frac{v_F^2q^2}{\omega_{p0}^2}+O(q^2)\right], \quad (17)$$

with

$$\tilde{F}(q)=-\tfrac{15}{16}(1+\epsilon_{\rm in}/\epsilon_{\rm sc})q/b-3(1-\epsilon_{\rm in}/\epsilon_{\rm sc})q/b+O(q^2).$$

The dotted line in Fig. 12 was calculated numerically. With increased surface-roughness scattering a minimum in the plasmon mass is found in Fig. 12, for the chosen parameters here, at $n\sim3\times10^{12}$ cm^{-2} for $\Delta=6$ Å. This behavior was seen in experiment.[15]

Let us mention that the increase of the plasmon mass at low density in Fig. 12 is mainly due to an M' effect, but the increase at high density is due to an M'' effect, as for a damped oscillator, in opposition to Ref. 14 where the low-density increase was explained as a damped oscillator effect. The increase at high density has been explained as multisubband effect,[16] but we cannot make a comparison with this theory because numerical values are not given there. However, our theory explains the increase in $M''(\Omega)/\Omega$ for high density found in experiment. A comparison of the relaxation time of plasmons from experiment and of the relaxation time in cyclotron-resonance experiments shows[57] that the magnetic field does not influence the relaxation kernel for $n>10^{12}$ cm^{-2}. This gives us a hint to forget about the magnetic field dependence of the current relaxation kernel in cyclotron-resonance experiments. The minimum in $M''(\Omega)/\Omega$ has also been found in experiment.[57] It has been pointed out in Ref. 15 that $\tau(\Omega)/\tau(0)<1$, and $\tau(0)$ is the dc relaxation time $1/M''(0)$. The origin of this behavior is the interaction effects in the current relaxation function (see Fig. 4).

The influence of $N_{\rm depl}$ on the plasmon mass is shown in Fig. 13 and is in qualitative agreement with experiment.[57] A finite depletion density increases the plasmon mass anomalies because of increased surface-roughness scattering and a greater insulating phase; see also Fig. 5(c).

In Ref. 17 it was argued that the onset of the mass enhancement at low density is correlated with the Fermi energy, when different surfaces with different valley degeneracies are compared. We cannot reproduce this in our theory (see Fig. 14), but we mention that there exists also a different transport mass in the different surfaces, and this is not taken into account in Fig. 14.

E. Cyclotron-resonance anomalies: Analytical results

In the following we discuss the conductivity in the presence of a magnetic field in the form given in Eq. (15a). With the approximation that $M_B(z)$ is independent from the magnetic field,[30]

$$M_B(z)=M(z), \quad (18)$$

we get

$$\sigma'(\omega,\omega_B)=\frac{ne^2}{m}M''(\omega)\frac{[\omega+M'(\omega)]^2+M''(\omega)^2+\omega_B^2}{\{[\omega+M'(\omega)]^2+M''(\omega)^2+\omega_B^2\}^2-4[\omega+M'(\omega)]^2\omega_B^2}. \quad (19)$$

The approximative equation (18) should only be meaningful for low magnetic field or dirty systems outside the region of the quantized Hall effect. For a magnetic field (ω_B) sweep, Eq. (19) can be discussed analytically. $\sigma'(\omega_B)$ has a max-

imum at a frequency ω_R and the magnetic fields of half-width at half maxima are ω_{H+} and ω_{H-}, respectively. From (19) one gets, with $\hat{\omega}_R=\omega_R/\omega$, $\hat{M}'=M'(\omega)/\omega$, and $\hat{M}''=M''(\omega)/\omega$,

$$\hat{\omega}_R^2=-[(1+\hat{M}')^2+\hat{M}''^2]+2\{(1+\hat{M}')^2[(1+\hat{M}')^2+\hat{M}''^2]\}^{1/2}\ , \tag{20}$$

with the asymptotic solution

$$\hat{\omega}_R^2=(1+\hat{M}')^2\left[1-\frac{\hat{M}''^4}{4(1+\hat{M}')^4}+O(\hat{M}''^6)\right],\quad \hat{M}''\ll|1+\hat{M}'| \tag{21a}$$

$$\hat{\omega}_R^2=\tfrac{3}{2}(1+\hat{M}')^2\left[1-\frac{\hat{M}''^2}{3(1+\hat{M}')^2}\right],\quad \hat{\omega}_R\ll 1\ . \tag{21b}$$

For $\hat{\omega}_{H\pm}=\omega_{H\pm}/\omega$ we get

$$\hat{\omega}_{H\pm}=(1+\hat{M}')^2\left\{4\left[\frac{1+\hat{M}''^2}{(1+\hat{M}')^2}\right]^{1/2}-2+\frac{1+\hat{M}''^2}{(1+\hat{M}')^2}\pm 2\left[3\frac{1+M''^2}{(1+\hat{M}')^2}+1-4\left[\frac{1+\hat{M}''^2}{(1+\hat{M}')^2}\right]^{1/2}\right]^{1/2}\right\}. \tag{22}$$

The half-width at half maxima $\Gamma_\pm$ of the resonance are given as

$$\Gamma_\pm=|\omega_{H\pm}-\omega_R|\ , \tag{23}$$

with the asymptotic solution

$$\Gamma_\pm=M''(\omega)\left[1+\frac{1}{4}\left[\frac{\hat{M}''}{1+\hat{M}'}\right]^2\pm\frac{1}{4}\left[\frac{\hat{M}''}{1+\hat{M}'}\right]^3+O(M''^4)\right],\quad \hat{M}''\ll|1+\hat{M}'| \tag{24a}$$

$$\Gamma_+=[\omega+M'(\omega)]\left[2+\left[5-4\frac{\hat{\omega}_R^2}{(1+\hat{M}')^2}\right]^{1/2}\right]^{1/2}-\omega_R,\quad \hat{\omega}_R\ll 1\ . \tag{24b}$$

For $M'=0$ we see from (21a) that the resonance frequency is reduced by dissipative effects. While this effect is quadratic in M'' for a harmonic oscillator, here it is proportional to $\hat{M}''^4$ because of the repulsion of the two resonances at $\pm\omega$. From (24a) we see that anomalies in the line shape should be an effect of order $\hat{M}''^3$, and these effects should channel in the full width at half maximum.

In Fig. 15 we have plotted $\hat{\omega}_R,\hat{\omega}_{H\pm}$ for $M'=0$ as function of $\hat{M}''(\omega)$. For $\hat{M}''>0.6$, $\Gamma_->1$ and the resonance structure is only weak. Let us mention only that the decrease of $\hat{\omega}_R$ for all $\hat{M}''$ comes from setting $\hat{M}'=0$ in Fig. 15. Departure from the lines in Fig. 15, when compared with experiments, can be interpreted as $M'(\omega)$ effects or as invalidity of the approximation, that the relaxation kernel is independent from the magnetic field. For the last interpretation, also, the sum rule

$$\int_{-\infty}^{\infty}d\omega_B\sigma'(\omega_B)=\pi ne^2/m\ , \tag{25}$$

valid for Eq. (19), could be invalid. Figure 15 is relevant in connection with the idea that the plasmon mass scales with $\omega\tau(\omega)=1/\hat{M}''(\omega)$. A scaling behavior with $\omega\tau(0)$ was found in experiment,[58] and first a mass increase and later a mass decrease with decreasing $\omega\tau(0)$ was reported. This is in qualitative agreement with our results and demonstrates the relevance of reactive effects from $M'(\omega)$.

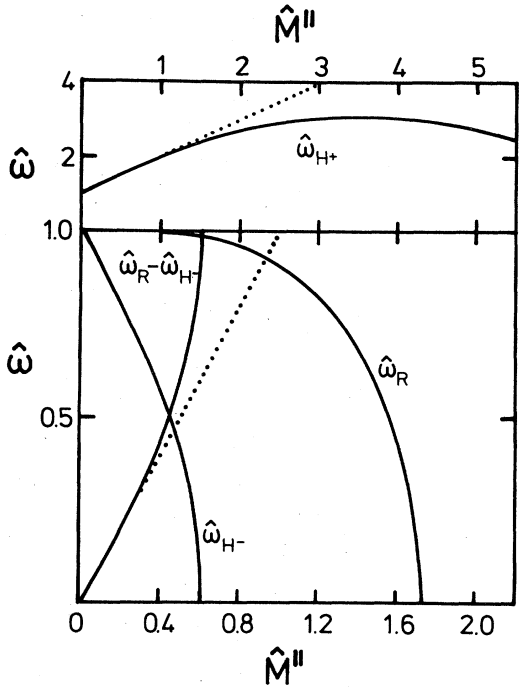

FIG. 15. $\hat{\omega}_R$, $\hat{\omega}_{H\pm}$, and $\hat{\omega}_R-\hat{\omega}_-$ as functions of $\hat{M}''$ according to Eqs. (20) and (22). The dotted lines are the asymptotic results for $\hat{M}''\ll 1$. For all curves, $\hat{M}'=0$.

F. Cyclotron-resonance anomalies: Numerical results

In Fig. 16 we have plotted $\sigma'(\omega)$ after Eq. (19) as a function of ω_B for various densities. The resonance positions are shown as arrows. From Eq. (21a) we expect the following behavior of the resonant magnetic field as a function of disorder. For small dissipative effects the shift of the resonance is determined by the sign of $M'(\omega)$, and because of interaction effects with positive $M'(\omega)$ we expect a shift to higher frequency (see Fig. 16). With increasing disorder (or decreasing density), M' changes sign and a shift to lower frequency happens. This effect is increased by dissipative effects due to M'', and the decrease of the resonance magnetic field happens already at somewhat higher density than where M' changes sign. The change of the resonance magnetic field can be interpreted as a cyclotron mass m^* via

$$m^* = m(\omega_R/\omega) , \tag{26}$$

and the behavior of m^* as a function of density is shown in Fig. 17. Such a behavior has been found in past experiments,[18,22] and in recent experiments where Na^+ ions as well-defined scattering centers were drifted to the interface.[19,59] The parameters of Fig. 17 have been chosen to explain the result (Fig. 5) of Ref. 19 quantitatively. The strong decrease of the resonance mass for low density may be interpreted as a localization precursor.[18,23] The increase of m^* with decreasing density was found before,[29,30] but there neutral-impurity scattering has been assumed. For increasing impurity concentration the cyclotron mass maximum decreases and goes to higher density.[19] m^*/m_0 becomes lower than 0.19 in the full density range shown in Fig. 17. The mass decrease for high density and high n_i was also seen in experiment.[19] A frequency dependence of the cyclotron mass has been reported as negligible.[60] In Fig. 18 we have plotted the cyclotron mass as function of density for various frequencies. For high frequency a broad density range is found where indeed m^* is independent of the frequency. For low frequencies a frequency dependence in qualitative ac-

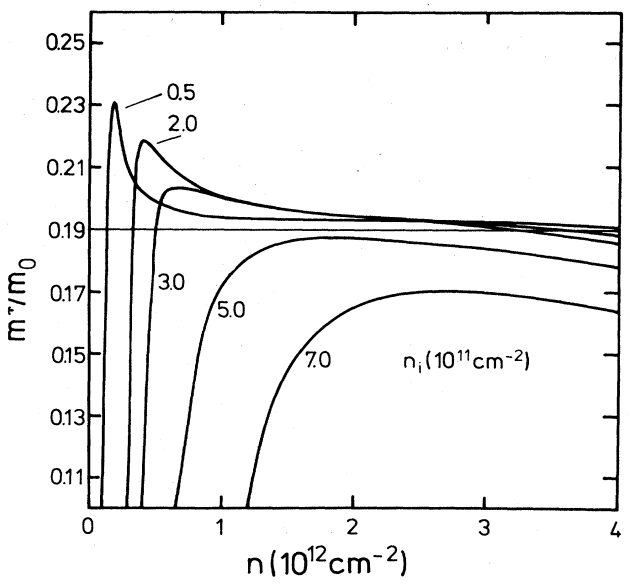

FIG. 17. Cyclotron mass as function of density according to our theory for $\omega = 3.68$ meV, $N_{\text{depl}} = 0$, $\Lambda = 30$ Å, and $\Delta = 4$ Å.

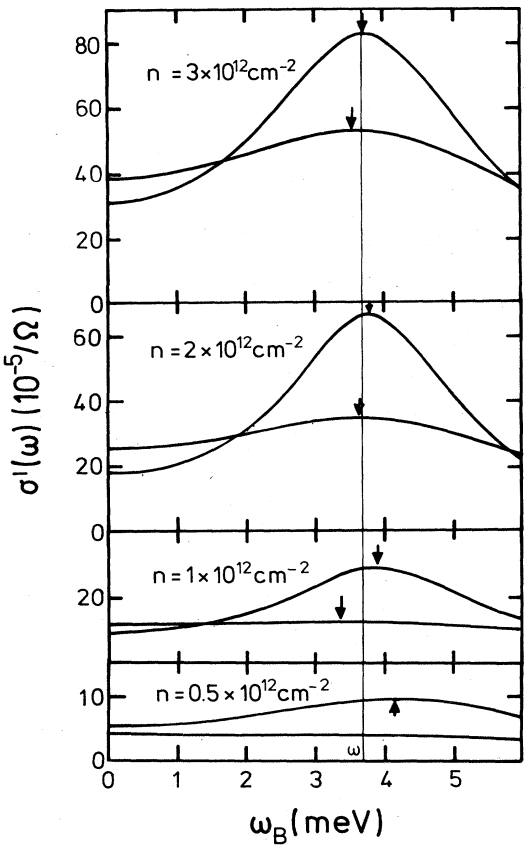

FIG. 16. Dynamical conductivity versus magnetic field according to our theory and Eq. (19) for different electron densities and $\Lambda = 30$ Å, $\Delta = 4$ Å, and $N_{\text{depl}} = 0$. The upper curves at $\omega_B = \omega$ are for $n_i = 0.6 \times 10^{11}$ cm^{-2} and the lower curves are for $n_i = 5 \times 10^{11}$ cm^{-2}. The arrows indicate the resonant magnetic fields ($\omega = 3.68$ meV).

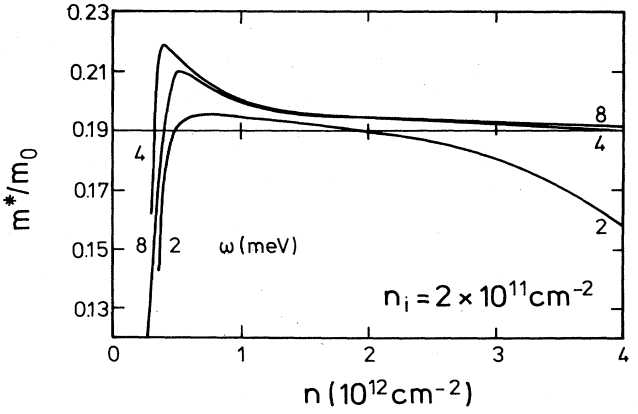

FIG. 18. Cyclotron mass versus density according to our theory for various frequencies and $N_{\text{depl}} = 0$, $\Lambda = 30$ Å, and $\Delta = 4$ Å.

cordance with our theory, see Fig. 18, was also found.[58] N_{depl} effects are shown in Fig. 19. The decrease of m^*/m_0 below 0.19 for high electron densities in Figs. 18 and 19 is due to dissipative effects, when surface-roughness scattering becomes the dominant scattering mechanism. Because the localized regime is increased by $N_{\text{depl}} \neq 0$, the decrease of m^* at low density begins at higher density for finite N_{depl} (see Fig. 19).

Until now we have discussed the behavior of the cyclotron mass in the good or poor metallic phase, but not yet in the insulator. There $M'(\omega) = -s/\omega$ for $\omega \to 0$ and s is the stiffness of the electron gas.[10] In $\sigma'(\omega)$ a quasigap exists for $0 < \omega < \omega_g$, with $M''(\omega) = 0$ because of level repulsion first discussed in Ref. 61 for a noninteracting electron gas. The correct result should be $\sigma'(\omega) \propto \omega^2 |\ln^3 \omega|$,[62] and is here[63] approximated by a quasigap. Then one expects, according to Eq. (20), a sharp resonance, broadened by temperature effects in the experiment, at frequencies

$$\omega_R = s/\omega - \omega \ . \tag{27}$$

The corresponding effective mass is shown in the left part of Fig. 20. This resonance should be accompanied by a drastic sharpening of the resonance. Such effects have been possibly seen in the experiment by Stallhofer *et al.*[64] and in Ref. 21.

Let us finally mention that in a frequency sweep of the conductivity, more anomalies in the line shape are expected, due to the strong frequency dependence of the relaxation kernel. For $\omega_B \gg |M(z)|$ one then expects the resonance at

$$\omega_R = \omega_B - M'(\omega_B) \ . \tag{28}$$

Thus the opposite sign of M' in comparison with the magnetic field sweep goes into the resonance shift. For high density with $M' > 0$ a decrease of the resonance is expected; later, when M' changes sign for decreasing n, an increase of the resonance should be found. In the strong insulator phase a sharp resonance is expected at

$$\omega = \omega_B/2 + (\omega_B^2/4 + s)^{1/2} \ . \tag{29}$$

Qualitatively, such a behavior as a function of density in a frequency sweep at fixed magnetic field has been found in Ref. 21, together with a strong narrowing of the resonance at low density. In light of our analysis, the suggestion in Ref. 65 for evidence of a magnetic-field-induced Wigner glass does not seem compulsory. The experiment may be

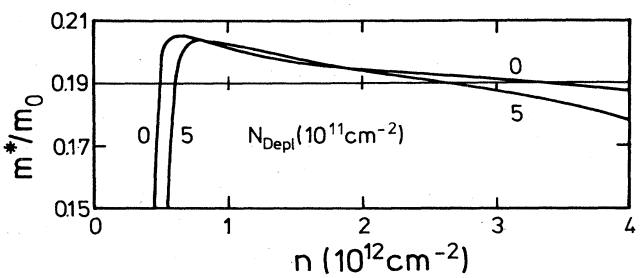

FIG. 19. Cyclotron mass versus density according to our theory for various values of N_{depl} and $\omega = 4$ meV, $n_i = 3 \times 10^{11}$ cm^{-2}, $\Lambda = 30$ Å, and $\Delta = 4$ Å.

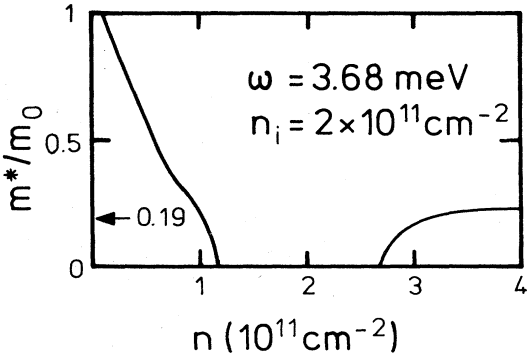

FIG. 20. Cyclotron mass versus density according to our theory for $N_{\text{depl}} = 0$, $\Lambda = 30$ Å, and $\Delta = 4$ Å.

understandable within our framework by a transition from a metallic electron gas to a localized Fermi glass. A more quantitative analysis of the experiment is in preparation.

V. CONCLUSIONS

The self-consistent current relaxation theory has been used to discuss static and dynamic properties of the conductivity with ionized-impurity scattering and surface-roughness scattering in MOS systems. Parameters for Si(100) have been used.

Peak mobility and density dependence of the mobility have been discussed in detail (Figs. 8 and 7). The plasmon decay channel of the current for the surface-roughness scattering was studied (Fig. 4). The influence of the current relaxation kernel on resonance experiments to study subband physics, plasmon anomalies, and magnetic field effects have been evaluated. The plasmon mass minimum found in the experiment has been explained by the existence of two scattering mechanisms (Fig. 12). The cyclotron mass increase and decrease found in the experiment have been interpreted quantitatively in terms of plasmon anomalies and a localization precursor, respectively (Fig. 17). A sharp cyclotron resonance is predicted in the insulator phase (Fig. 20).

The theory gives for the first time a unified picture of static and dynamic properties of a strong, disturbed two-dimensional electron gas. Mobility peak, cyclotron mass maximum, and plasmon mass minimum[63] are the result of the interplay of ionized-impurity scattering and surface-roughness scattering within a nonlinear scattering theory and the frequency dependence of the current relaxation rate.

ACKNOWLEDGMENTS

I would like to thank Professor F. Koch for many helpful discussions in connection with the status of the cyclotron-resonance anomalies. Useful discussions with Dr. G. Abstreiter, Dr. D. Heitmann, Professor K. v. Klitzing, Professor J. P. Kotthaus, and C. Mazuré are also acknowledged. This work was supported by the Deutsche Forschungsgemeinschaft (DFG) via Sonderforschungsfereich (SFB) 128.

[1]T. Ando, A. B. Fowler, and F. Stern, Rev. Mod. Phys. **54**, 437 (1982).
[2]F. Stern and W. E. Howard, Phys. Rev. **163**, 816 (1967).
[3]R. F. Greene, in *Molecular Processes on Solid Surfaces,* edited by E. Dranglis, R. D. Gretz, and R. I. Jaffee (McGraw-Hill, New York, 1969), p. 239.
[4]Y. C. Cheng, in *Proceedings of the Third Conference on Solid State Devices, Tokyo, 1971* [Suppl. J. Jpn. Soc. Appl. Phys. **41**, 173 (1972)].
[5]Y. C. Cheng and E. A. Sullivan, Surf. Sci. **34**, 717 (1973).
[6]Y. Matsumoto and Y. Uemura, in *Proceedings of the Second International Conference on Solid Surfaces, Kyoto, 1974* [Jpn. J. Appl. Phys. Suppl. 2, Pt. 2, 367 (1974)].
[7]F. Stern, Surf. Sci. **73**, 197 (1978).
[8]S. J. Allen, D. C. Tsui, and F. De Rosa, Phys. Rev. Lett. **35**, 1359 (1975).
[9]A. Gold, S. J. Allen, B. A. Wilson, and D. C. Tsui, Phys. Rev. B **25**, 3519 (1982).
[10]W. Götze, Solid State Commun. **27**, 1393 (1978).
[11]P. W. Anderson, Phys. Rev. **109**, 1492 (1958).
[12]S. J. Allen, D. C. Tsui, and R. A. Logan, Phys. Rev. Lett. **38**, 980 (1977).
[13]F. Stern, Phys. Rev. Lett. **18**, 546 (1967).
[14]G. F. Giuliani and J. J. Quinn, Phys. Rev. B **29**, 2321 (1984).
[15]D. Heitmann, J. P. Kotthaus, and E. G. Mohr, Solid State Commun. **44**, 715 (1982).
[16]S. Das Sarma, Phys. Rev. B **29**, 2334 (1984).
[17]E. Batke and D. Heitmann, Solid State Commun. **47**, 819 (1983).
[18]J. P. Kotthaus, G. Abstreiter, J. F. Koch, and R. Ranvaud, Phys. Rev. Lett. **34**, 151 (1975).
[19]H. R. Chang and F. Koch, *Lecture Notes in Physics* (Springer, Berlin, 1983), Vol. 177, p. 127.
[20]T. A. Kennedy, R. J. Wagner, B. D. McCombe, and D. C. Tsui, Solid State Commun. **21**, 459 (1977).
[21]B. A. Wilson, S. J. Allen, and D. C. Tsui, Phys. Rev. Lett. **44**, 479 (1979).
[22]G. Abstreiter, J. P. Kotthaus, J. F. Koch, and G. Dorda, Phys. Rev. B **14**, 2480 (1976).
[23]H. J. Mikeska and H. Schmidt, Z. Phys. B **20**, 43 (1975).
[24]C. S. Ting, S. C. Ying, and J. J. Quinn, Phys. Rev. B **16**, 5394 (1977).
[25]A. W. Overhauser, Phys. Rev. B **18**, 2884 (1978).
[26]B. E. Sernelius and K. F. Berggren, Surf. Sci. **98**, 191 (1980).
[27]W. Götze and J. Hajdu, Solid State Commun. **29**, 89 (1979).
[28]W. Götze and P. Wölfle, Phys. Rev. B **6**, 1226 (1972).
[29]A. Isihara and M. Mukai, Phys. Rev. B **24**, 7408 (1981).
[30]A. Isihara and M. Mukai, Phys. Rev. B **28**, 4842 (1983).
[31]A. Gold and W. Götze, Solid State Commun. **47**, 627 (1983).
[32]A. Gold and W. Götze (unpublished).
[33]N. Tzoar, P. N. Platzmann, and A. Simons, Phys. Rev. Lett. **36**, 1200 (1976).
[34]C. S. Ting, T. K. Lee, and J. J. Quinn, Phys. Rev. Lett. **34**, 870 (1975).
[35]H. R. Chang and F. Koch, Surf. Sci. **113**, 144 (1982).
[36]A. Gold, W. Götze, C. Mazuré, and F. Koch, Solid State Commun. **49**, 1085 (1984).
[37]A. Hartstein, A. B. Fowler, and M. Albert, Surf. Sci. **98**, 181 (1980).
[38]A. Gold, Phys. Rev. Lett. **54**, 1079 (1985).
[39]F. F. Fang and W. E. Howard, Phys. Rev. Lett. **16**, 797 (1967).
[40]T. Ando, J. Phys. Soc. Jpn. **43**, 1616 (1977).
[41]In Eq. (2.29b) of Ref. 40, $\arctan[(q/b-1)/(q/b+1)]$ must be replaced by $\arctan[\sqrt{q/b-1}/\sqrt{q/b+1}]$.
[42]D. Pines and P. Nozières, *The Theory of Quantum Liquids* (Benjamin, New York, 1966).
[43]M. Jonson, J. Phys. C **9**, 3059 (1976).
[44]W. Götze, Philos. Mag. B **43**, 219 (1981).
[45]A. Gold and W. Götze, J. Phys. C **14**, 4049 (1981).
[46]R. E. Prange and T. W. Nee, Phys. Rev. **168**, 779 (1968).
[47]B. T. Moore and D. K. Ferry, J. Vac. Sci. Technol. **17**, 1037 (1980).
[48]Y. Kawaguchi, T. Suzuki, and S. Kawaji, Surf. Sci. **113**, 218 (1982).
[49]E. Voss, R. Lassing, and E. Gornik, Surf. Sci. **113**, 223 (1982).
[50]S. M. Goodnick, R. G. Gann, D. K. Ferry, C. W. Wilmsen, and O. L. Krivanek, Surf. Sci. **113**, 233 (1982).
[51]P. O. Hahn and M. Henzler, J. Appl. Phys. **54**, 6492 (1983).
[52]V. B. Timofeev (private communication).
[53]K. v. Klitzing (private communication).
[54]C. Mazuré, F. Martelli, A. Gold, U. Grzesik, H. R. Chang, and F. Koch, Solid State Commun. **54**, 443 (1985).
[55]A. Gold (unpublished).
[56]T. Ando, Z. Phys. B **26**, 263 (1977).
[57]E. Batke and D. Heitmann (unpublished).
[58]T. A. Kennedy, R. J. Wagner, B. D. McCombe, and D. C. Tsui, Phys. Rev. Lett. **35**, 1031 (1975).
[59]F. F. Fang, A. B. Fowler, and A. Hartstein, Phys. Rev. B **16**, 4446 (1977).
[60]G. Abstreiter, F. Koch, P. Goy, and Y. Gouder, Phys. Rev. B **14**, 2494 (1976).
[61]W. Götze, J. Phys. C **12**, 1279 (1979).
[62]N. F. Mott and E. A. Davies, *Electronic Processes in Non-Crystalline Materials* (Clarendon, Oxford, 1979).
[63]A. Gold, dissertation, Technische Universität München, 1984.
[64]P. Stallhofer, J. P. Kotthaus, and F. Koch, Solid State Commun. **20**, 519 (1976).
[65]B. A. Wilson, S. J. Allen, and D. C. Tsui, Phys. Rev. B **24**, 5887 (1981).